Passive RFID at Millimeter Waves

Pekka Pursula, *Member, IEEE,* Francesco Donzelli, Heikki Seppä

***Abstract*— This paper introduces a novel way to implement passive RFID at millimeter waves. The passive operation is achieved by adding an external mixing element between tag antenna and a standard RFID chip. The mixing element converts RFID reader signal from millimeter waves to RFID carrier frequency – the RFID chip operates as usual. Either passive or semipassive RFID circuits, at any RFID carrier frequency can be used. The reader's TX and RX ports are similarly equipped with external mixers to convert the reader output to millimeter waves and received millimeter wave signal to RFID carrier frequency. The paper analyses the concept theoretically with a Schottky diode as the mixing element. The design and experimental demonstration of the operation at 10 GHz are presented. Using an EPC-compliant UHF tag IC and reader, a range of 30 cm is demonstrated, but range extension to over a meter is feasible.**

***Index Terms*—Radio frequency Identification, RFID, Millimeter wave identification, MMID.**

I. INTRODUCTION

Radio frequency identification (RFID) has gained a lot of attention recently. Passive RFID technology at UHF has enabled several applications, e.g. in tracking of goods in supply chain, and asset management. The success of the technology is based on robust identification with inexpensive (even less than 10 Euro cent) tags, and standards ([1],[2]) that guarantee the interoperability of tags and readers of different manufacturers.

UHF RFID delivers a range of even 10 meters, but it lacks efficient locating capabilities within the reader. Both received signal strength (RSSI, e.g. [3]) or phase (e.g. [4],[5]) has been used for ranging the tags, but these methods do not address the direction of the tag, but only the range. Finding the direction of the tag would require either multiple antennas and trilateration or a narrow-beamed, i.e. highly directional reader antenna. The directional antenna would be overwhelmingly large at UHF, but at millimeter waves a directional antenna can be realized in practical dimensions.

Millimeter wave RFID, or MMID, provides also higher data rates due to more relaxed radio regulations e.g. at 60 GHz [6], and miniaturized reader and tag antennas [7]. The drawback is that the antenna effective aperture scales in the square of the wavelength, effectively diminishing the available power in the passive tag.

The key component in the passive tag operation is the rectifier in the tag. Rectification at low power levels is inefficient. At UHF, rectifier efficiencies of 60 % are reported [8]. Scaling of CMOS to higher frequencies has enabled integrated rectifiers at millimeter waves, too. In [9], an integrated mm-wave RFID tag at 60 GHz is reported with rectifier efficiency of 1.2 %. However, the protocol in the tag is sequential, limiting the data rate to 5 kb/s.

In this paper, we present an alternative solution for using millimeter waves for RFID. We propose using an external nonlinear component between tag antenna and RFID chip for mixing millimeter waves to RFID carrier frequency for a standard RFID chip, as illustrated in Fig. 1.

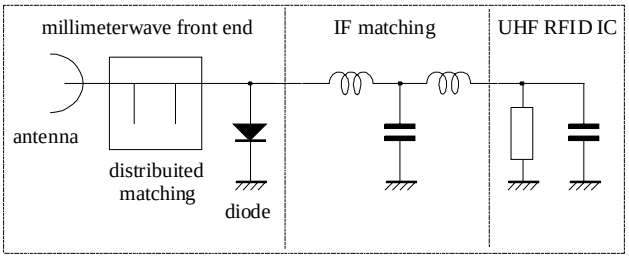

Fig. 1 The block diagram of the proposed millimeter wave RFID tag.

The tag receives a millimeter wave carrier at ω_0 with the UHF RFID signal in sidebands at $\omega_0 \pm \omega_{IF}$, where ω_{IF} is a frequency in the UHF RFID range (850-950 MHz). The received signal is down-converted in the external mixing element (here a diode) to ω_{IF}. This UHF signal is then fed to the UHF RFID chip, which operates as usual. Modulation of the RFID chip at $\omega_{IF} \pm \omega_{mod}$ propagates similarly through the mixing element to frequencies $\omega_0 \pm \omega_{IF} \pm \omega_{mod}$, which are then transferred through the tag antenna to the reader receiver antenna.

The reader consists of a standard UHF RFID reader, whose TX/RX output is connected to a circulator. The TX signals are up-converted in an external mixer to millimeter waves, amplified and fed to a millimeter wave antenna. The transmission includes the millimeter carrier frequency ω_0 and sidebands at $\omega_0 \pm \omega_{IF.}$ The received signal is similarly down-converted by an external mixer to $\omega_{IF} \pm \omega_{mod}$, which is fed to the standard UHF RFID reader.

The system enables passive RFID at millimeter waves with

Pekka Pursula and Heikki Seppä are with VTT Technical Research Centre of Finland, P.O.Box 1000, FI-02044 VTT, Espoo, Finland. Correspondence to pekka.pursula@vtt.fi.

Francesco Donzelli is with the DEIS, University of Bologna, 40136 Bologna, Italy (e-mail: francesco.donzelli@unibo.it).

standard EPC protocol, including all the features of the UHF RFID, such as anticollision, data rates, etc. In this paper, operation is demonstrated at 10 GHz, but the idea works at any carrier frequency substantially higher than the frequency of the RFID chip. Also HF RFID chips could be used, but their power consumption is higher than UHF chips, leading to even shorter range. On the other hand, semipassive UHF RFID chips have better sensitivity than passive ones, which would enable higher range.

In this paper we use a Schottky diode as the mixing element at the tag, but other possibilities exists. Capacitive mixer components, such as varactor diodes, ferroelectric varactors or even MEMS resonators could diminish theconversion loss, but no suitable commercial components exist at millimeter waves [10].

The paper is structured as follows. The next chapter analyses the operation principle of the tag theoretically. Detailed simulation and design of the demonstrator tag at 10 GHz including range estimation is presented in Chapter III, and experimental verification in Chapter IV.

II. THEORY

Theoretical analysis of the tag can be divided to two separate parts by assuming that the millimeter wave matching circuit presents a high impedance at UHF, and vice versa. We model the diode as an ideal nonlinear resistor with

$$I_D = I_0\left(e^{qV_D/nkT} - 1\right). \tag{1}$$

Further, we assume constant diode capacitance, which can be hence bundled within the matching networks in the following analysis. Omitting the reactive matching, which is assumed ideal, the tag can be presented by the model in Fig. 2. This simple model is enough to illustrate the operation principle of the external mixing element. In practice, the nonlinear capacitance also affects the results, and it is taken into account in the detailed simulation in the next Chapter.

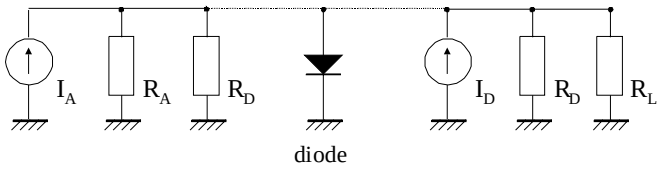

Fig. 2 The circuit schematic for theoretical analysis.

A. Power conversion efficiency in forward link

The antenna is modeled as a current source I_A with internal resistance R_A. The antenna receives three tones from the reader device: Carrier at ω_0 and sidebands at $\omega_0 \pm \omega_{IF}$. The antenna works as an efficient bandpass filter, and only carrier at ω_0 and upper sideband at $\omega_0 + \omega_{IF}$ propagate to the diode. Hence the antenna current is written as

$$I_A = A_1 \sin(\omega_0 t) + A_2 \sin\left((\omega_0 + \omega_{IF})t\right). \tag{2}$$

The voltage over the diode is

$$V_D = \frac{R_A R_D}{R_A + R_D} I_A = \frac{R_D}{2} I_A, \tag{3}$$

where the latter equality maximizes the voltage at conjugate match, i.e. $R_A = R_D$.

At the UHF circuitry, the diode is modeled as a current source, defined by the Taylor expansion of the ideal diode I-V –curve of Eq. (1).

$$I_D = I_{D0} + \left(\frac{\partial I_D}{\partial V_D}\right) V_D + \frac{1}{2}\left(\frac{\partial^2 I_D}{\partial V_D^2}\right) V_D{}^2. \tag{4}$$

Assuming zero DC bias ($I_{D0} = I_0$), we get to the second order

$$\begin{aligned} I_D = I_0 &+ \frac{A_1}{2}\sin(\omega_0 t) + \frac{A_2}{2}\sin\left[(\omega_0 + \omega_{IF})t\right] \\ &+ \frac{1}{2^3} R_D \gamma \{A_1{}^2 + A_2{}^2 - A_1{}^2 \cos(2\omega_0 t) \\ &\quad - A_2{}^2 \cos\left[2(\omega_0 + \omega_{IF})t\right] + 2A_1 A_2 \cos(\omega_{IF} t)\}. \end{aligned} \tag{5}$$

Here we have used the relations

$$R_D = \left(\frac{\partial I_D}{\partial V_D}\right)^{-1}, \qquad \gamma = \left(\frac{\partial^2 I_D}{\partial V_D^2}\right) \Big/ \left(\frac{\partial I_D}{\partial V_D}\right) \tag{6}$$

The interesting terms in Eq. (4) are the DC term and the last term at ω_{IF}. To find out the DC operating point of the diode for evaluating the derivatives in Eq. (4), one must take into account the DC created by the diode. This could be done in any circuit analysis software, and is taken into account in the following simulations, but for now we only state that the derivatives are evaluated at the DC operating point.

The UHF signal that will be delivered further by the UHF matching network is the term

$$I_D = \frac{1}{4} R_D \gamma A_1 A_2 \cos(\omega_{IF} t). \tag{7}$$

Hence the power delivered to load R_L is

$$P_L = R_L \left(\frac{1}{1 + R_L/R_D} |I_D|\right)^2 = \frac{A_1{}^2 A_2{}^2}{2^7} R_D{}^3 \gamma^2 \tag{8}$$

at conjugate match. This is maximized when $A_1 = A_2$, which gives for the power P_A available from the reader field

$$P_A = R_A \left(\frac{1}{1 + R_A/R_D} |I_A|\right)^2 = \frac{A_1{}^2 R_D}{2^2}. \tag{9}$$

Forward link conversion efficiency α_f is the ratio of P_L to the power P_A available from the reader field

$$\alpha_f = \frac{P_L}{P_A} = \frac{A_1^2}{2^5} R_D^2 \gamma^2 = \frac{P_A}{2^3} R_D \gamma^2 \quad (10)$$

The latter term illustrates that the conversion efficiency is directly proportional to the input power.

B. Return link

Communication in the return link is based on backscattering modulation. The UHF RFID chip modulates its input impedance, in this model its resistance by a value of ΔR_L. The modulation in the chip resistance is seen as a change in the voltage over the diode

$$V_D = \Delta R_L \left(\frac{\partial}{\partial R_L} \frac{R_D R_L}{R_D + R_L} \right) I_D = \frac{1}{2^4} R_D^2 \gamma \frac{\Delta R_L}{R_L} A_1 A_2 \cos(\omega_{IF} t), \quad (11)$$

where the latter equality follows from evaluating the derivative at the complex conjugate match. This voltage represents a third input voltage for the diode, leading to new output current components from the diode nonlinearity. Using similar analysis as in the forward link case in Eqs.(4)-(6), we get the output current component at $\omega_0 + \omega_{IF}$

$$I_D = \frac{1}{2^5} R_D^2 \gamma^2 \frac{\Delta R_L}{R_L} A_1^2 A_2 \cos[(\omega_0 + \omega_{IF})t]. \quad (12)$$

Similarly to Eq. (8), the power delivered to antenna at conjugate match is

$$P_{A,return} = \frac{A_1^4 A_2^2}{2^{13}} R_D^5 \gamma^4 \left(\frac{\Delta R_L}{R_L} \right)^2. \quad (13)$$

The return link power conversion efficiency α_r is the ratio of the power returned to the antenna $P_{A,return}$ and the power P_A available from the reader field, evaluated at the optimal power condition of the forward link, i.e. $A_1 = A_2$

$$\alpha_r = \frac{P_{A,return}}{P_A} = \frac{P_A^2}{2^7} R_D^4 \gamma^4 \left(\frac{\Delta R_L}{R_L} \right)^2 = \frac{1}{2} \left(\frac{\Delta R_L}{R_L} \right)^2 \alpha_f^2. \quad (14)$$

The return link power conversion efficiency is proportional to the forward link conversion efficiency squared and the modulation index $\Delta R_L/R_L$ squared. Hence the diode attenuates the incoming and outgoing signals equally, as does the free space between the reader and the tag.

III. Simulations

A. Antenna design

The necessity to operate at microwave frequencies force us to operate as follows: at the transmitter side a baseband AM-modulated signal will be produced by an ordinary DSP-based RFID reader and internally up-converted to ω_{IF} among a range of 850 - 950 MHz. Then an external customized mixer will perform the follow-up conversion to $\omega_0 \pm \omega_{IF}$ by a suitable oscillator tone ω_0 – at 10 GHz in this case – at the end of our reading block scheme.

The double up-conversion architecture implies a relative transmitted signal bandwidth of ω_{IF}/ω_0 = 10 % at least - by means of a suitable image-rejection mixer - and the necessity to count on huge-bandwidth antennas. An endfire traveling-wave Vivaldi planar topology was preferred due to its simple structure, high gain, good efficiency and wide band. Its working mechanism consisting of a slotline flared outward to an aperture where the wave impedance matches free-space was firstly described by [11]. The most critical elements for the antenna performances such as microstrip-to-slotline transition and exponential tapered parts have been analyzed and refined by full-wave EM simulation [12] through the Method of Moments technique. The layout is shown in Fig. 3 while in Fig. 4 a comparison can be appreciated between simulated and measured Return Loss. The substrate is Rogers RO4350B (h = 0.762 mm, Cu ½ oz, ε_r = 3.66, tanδ = 0.004).

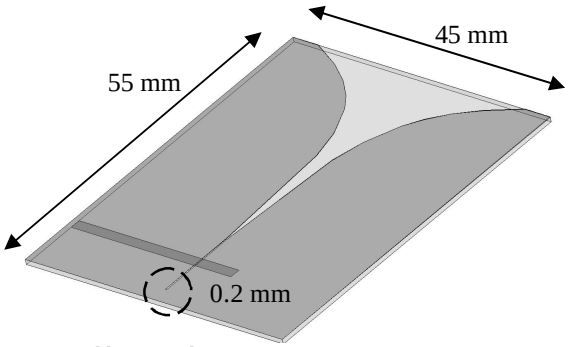

Fig. 3 Vivaldi antenna layout.

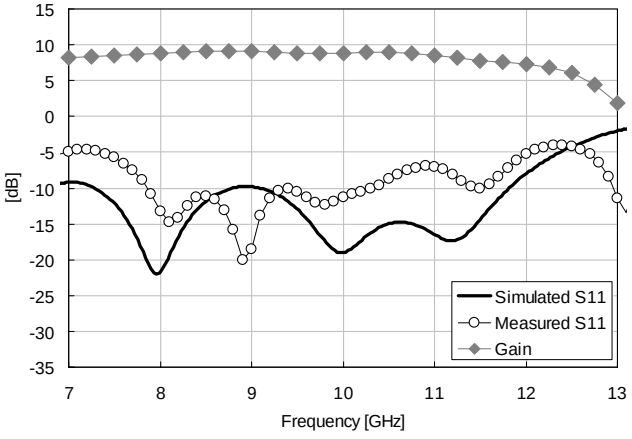

Fig. 4 Antenna Return Loss and Gain

B. Front-end design considerations

Since the ordinary RFID chip is expected to be operating at UHF (850 - 950 MHz), the tag working principle will basically consist of a nonlinear harmonic generation provided

by a single-diode mixer - simplest and most effective topology in the present case - with local oscillator tune furnished by the incoming continuous wave at ω_0 from the transmitter: the load will be only interested by the intermodulation product at ω_{IF} at the chip's side. A key feature in the mixer design is the choice for a suitable diode, in this case an Avago Technologies HSMS-286B (C_{J0} = 0.18 pF, I_S = 50 nA, N = 1.08 and V_J = 0.65 V); then a suitable matching section between antenna and nonlinear device should be included and refined by means of Conversion Loss optimization goal [13]. The simulations take fully into account also the nonlinear capacitance of the diode.

Inside the optimization loop without any loss of generality we will assume that the two driving tunes are sinusoidal, with incommensurate fundamental frequencies ω_0 and ω_{RF}. A minimum power of -14 dBm at ω_{IF} is required for the selected RFID IC - Alien Technologies Higgs 2 - in the acknowledgement phase. A block diagram of the tag is presented in Fig. 5 and a photograph of the tag in Fig. 6.

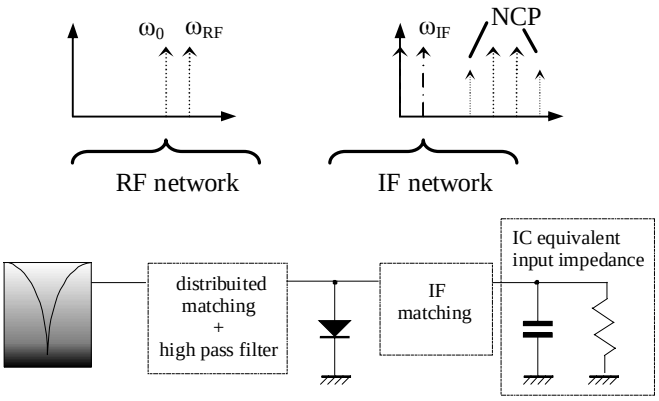

Fig. 5 Front-end block diagram.

The whole front-end can be roughly divided into two distinct subnetworks according to the respective working frequencies: the first one, depicted as RF network, provides for a conjugate matching between antenna and front-end in the neighborhood of the carrier wave – thus considering ω_{IF} as generically comprised in a range of 850 - 950 MHz depending on the communication protocol standard; at the same time a High Pass Filter (HPF) at 9.1GHz is inserted to operate in conjunction with the antenna return loss for bouncing the consistent near-carrier intermodulation products (NCP in the picture) between antenna itself and IF network. Inserted to remix NCP's at the diode and thus form more IF power, HPF is simply realized by a shunt short-stub followed by a microstrip line.

The lumped Tee section is introduced as a band-stop filter for 10 GHz harmonic, exploiting inductors' self resonances – in this case 12 and 5.5 GHz respectively. Final values for the three lumped elements are 3.3 nH, 4.3 nH and 1.5 pF respectively.

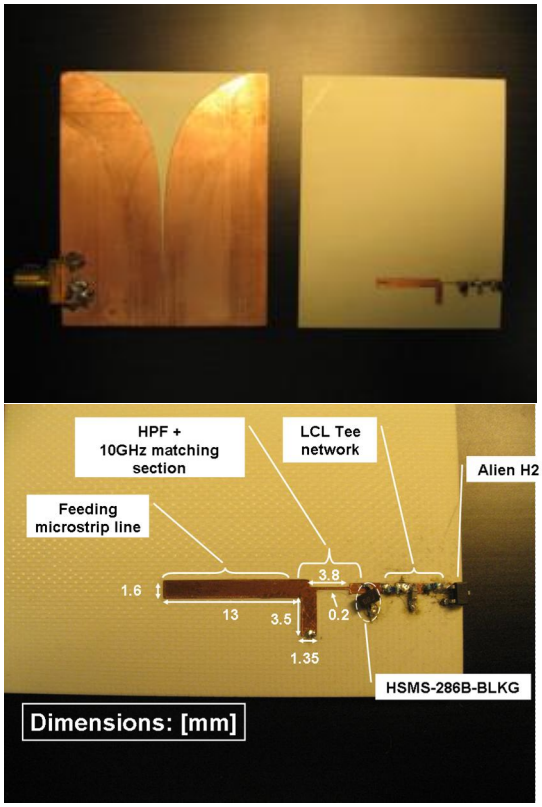

Fig. 6. Final Tag detailed view

To the authors' experience a lumped shunt RC equivalent circuit is sufficient to model the electrical chip behaviour: in this case the nominal values of R = 1500 Ω and C = 1.2 pF were assigned and then successfully checked.

All the blocks have been modeled and refined by a unique optimization loop: all the parasitic effects due to diode package 0201 are taken into account. The entire front-end is totally passive. The simulated conversion loss is given in Fig. 7.

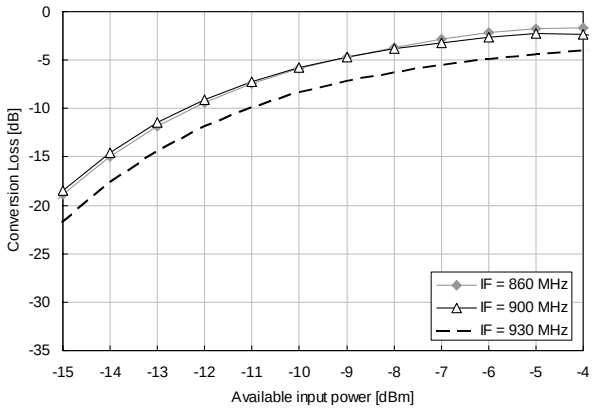

Fig. 7. Estimated conversion loss at different frequencies and input power levels.

C. *Range estimation*

An accurate evaluation of the power available to the IC is developed by combining the reciprocity theorem with the

antenna performances, computed by electromagnetic (EM) simulation [14]. Such approach was demonstrated to be able to avoid some ineffectiveness of a mere Friis equation in the case the far-field assumption in the link analysis between Reader and Tag is disregarded (e.g. dist < 10 λ, with λ as free-space-wavelength at the frequency of interest). Furthermore, port mismatch and power transfer effects between the antenna elements and the nonlinear subsystems are now rigorously accounted for [15]. Following the classic EM formalism to specify a field source in terms of known current source we can still refer to the Norton-equivalent representation for the entire circuit schematic as depicted in Fig.2.

The current source I_A (ω) - depending only on the electric field $\mathbf{E_T}$ of the incoming plane wave (IPW) from the transmitter - plays the role of free source in the receiver analysis and can be computed in two steps: first the incident field is temporarily suppressed and the receiving antenna is employed in a transmitting mode. Through an arbitrary excitation by a current density I injected at the input port, the antenna can be analyzed by a commercial 3-D EM simulator [12] in order to derive both the radiated far field distribution and the frequency-dependent antenna admittance $Y_A(\omega)=[R_A(\omega)]^{-1}$ at all the frequencies of interest. If we denote the former by $\mathbf{E_R}(r_A,\theta_A,\phi_A;\omega)$ in a suitable receiver-referred spherical reference frame, the result from EM analysis would be generally the complete set of the scalar components of the normalized field $\mathbf{E_{Rn}}(\theta_A,\phi_A;\omega)$

$$\mathbf{E_{Rn}}(\theta_A,\phi_A;\omega)=r_A\cdot exp(j\beta r_A)\frac{\mathbf{E_R}(r_A,\theta_A,\phi_A;\omega)}{I}, \qquad (15)$$

where r_A is the generic distance at which $\mathbf{E_R}$ is evaluated.

As a second step, the antenna is used in a receiving mode in the presence of $\mathbf{E_T}$, so that by Eq. (16) coincides with the port current. A straightforward application of the reciprocity theorem leads to the following form generated by the relationship between the fields and associated currents:

$$I_A(\omega)=j\frac{2}{\eta}\lambda Y_A(\omega)\cdot \cdot\mathbf{E_{Rn}}(\theta_A,\phi_A;\omega)\bullet\mathbf{E_T}(r,\theta_I,\phi_I;\omega), \qquad (16)$$

where r is the read range, (θ_I, φ_I) the angular coordinates of the direction of incidence of $\mathbf{E_T}$ in its respective reference frame (usually different from the receiver-referred one) and η is the free-space impedance. It is noteworthy to mention that such current source I_A is independent from the excitation I and is only a function of the IPW field and direction of incidence.

By means of such approach a first evaluation of the effective read range can be performed by starting from some average values of radiated power from the transmitter: with 23 dBm ERP the required -14 dBm power level to the Alien chip can be guaranteed at about 15 cm distance. At the same distance by making use of Eq. (14) the backscattered signal power is proven to fulfill a standard reader sensitivity of roughly -80 dBm – a huge noise contribution among the entire block chain should be considered.

Of course the read range might be considerably increased through a suitable active device at the reader side, such a high-gain power amplifier. Increasing the TX power to 30 dBm ERP, the range would extend to 30 cm. Adding a higher gain tag antenna, e.g. a 2*2 patch antenna array gives a 4-fold gain, or 2-fold range compared to a single patch, or a Vivaldi. The array is similar to UHF RFID tag antennas in size (5*5 cm^2). Further, using a semipassive tag IC, the tag sensitivity could be reduced at least 12 dB. Because the conversion loss also scales in the incoming power, this would only give two-fold range extension. Hence the range can be extended to over a meter. Capacitive mixing might help to extend the range further, especially with the extremely low input power of semipassive UHF RFID tags.

IV. Measurements

A. Forward link performance

The forward link conversion loss was measured by means of a continuous wave feeding system: a block scheme is given in Fig. 8, with the authentic tag load replaced by the 50-Ω spectrum analyzer input impedance. For the measurement, a new matching network at IF was implemented (L_1 = 3.3 nH, L_2 = 22 nH, C = 4.6 pF) to match the 50-Ω load to the diode.

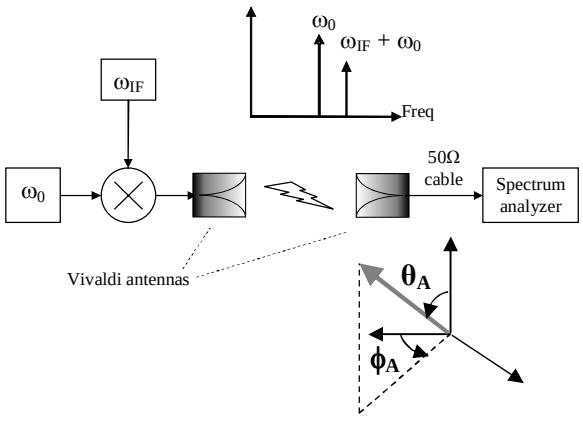

Fig. 8. Forward link measurement setup.

In the measurements, the power of the carrier at ω_0 and the upper sideband $\omega_0 + \omega_{IF}$ were tuned to -10 dBm at the diode input. The lower sideband at $\omega_0 - \omega_{IF}$ was not considered relevant, because the tag antenna and millimeter wave filter attenuates it significantly. Hence the lower sideband power was allowed to vary a few dB, in order to keep the carrier and upper sideband powers constant. The measured conversion loss is presented in Fig. 9 as a function of IF frequency.

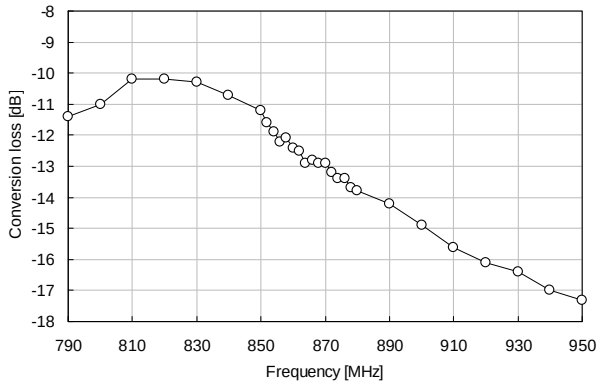

Fig. 9. Measured conversion loss of the diode at -10 dBm input power at carrier and upper sideband as a function of the IF frequency.

The IF matching is at its best at 820 MHz, were a conversion loss of about -10 dB is achieved. The conversion loss at the nominal operation frequency of 860 MHz is 2.2 dB lower. Power sweep measurement in Fig. 10 was carried out at the nominal operation frequency of 860 MHz. The theoretical curve is calculated for the diode with R_D = 6 Ω (zero DC bias), taking into account the suboptimal IF matching at 860 MHz by subtracting 2.2 dB from the theoretical value given by Eq. (10). The measured conversion loss is in line with the theory at low input power. Hence the capacitive mixing in the diode seems not to be of high importance in the demonstrator system. Of course, the small signal model of Chapter II cannot predict the saturation, but the simulations in Fig. 7 and the measurements show a similar saturation behavior. However, the measurements exhibit higher conversion loss, most probably due to the fact that the IF matching is not at its best at 860 MHz – this is also seen in the simulations, where the conversion loss at 930 MHz – 70 MHz above the nominal IF matching frequency – shows a flatter power response.

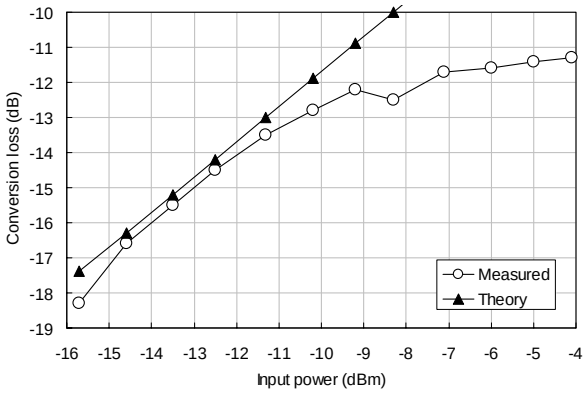

Fig. 10. Measured conversion loss of the diode at 860 MHz IF frequency as a function of the input power at carrier and upper sideband.

B. *Full operation*

Finally a full system as depicted in Figs. 11 and 12 was constructed for determining the actual read range: for sake of simplicity two-element Vivaldi array is employed as a transceiver at the reading side. Setup enhancements include two high-gain power amplifiers positioning (Quinstar QPJ and Miteq JS4) and tuning of reader RX and TX antenna separation as well as reader output power control at the RFID reader in order to keep the optimum feeding condition $A_1 = A_2$ (see Chapter II.A). The transmit power in the measurement is about 30 dBm ERP along all the frequency range.

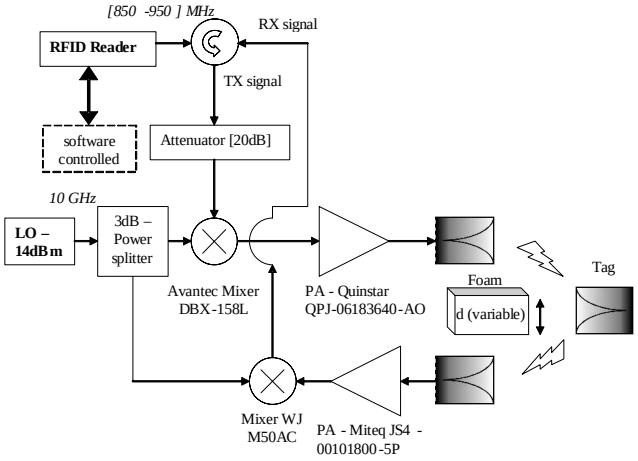

Fig. 11. Read range measurement setup schematic.

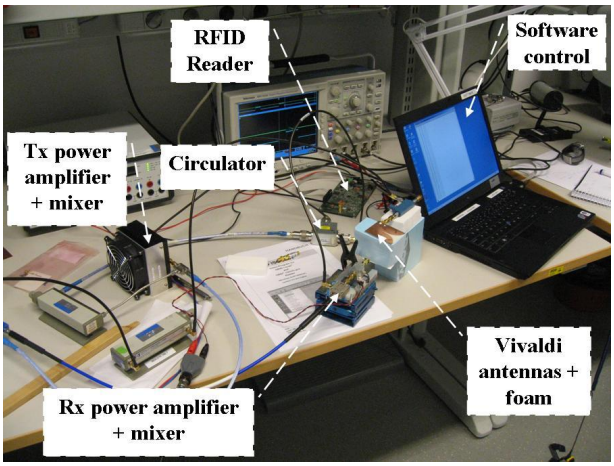

Fig. 12. Read range measurement setup photograph.

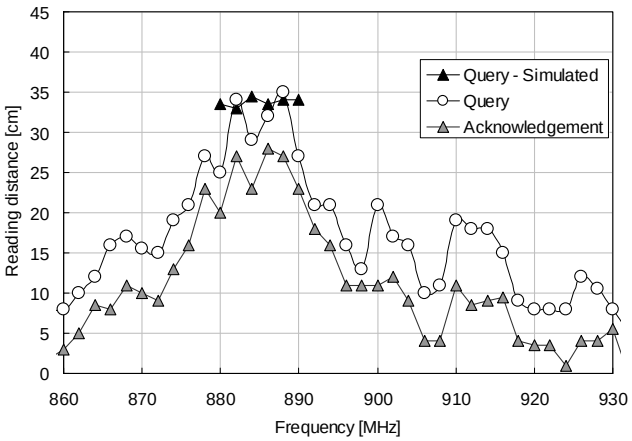

Fig. 13. Measured read range as a function of IF frequency.

The measured tag range was about 30 cm. About 5 cm longer range was observed with the first query of the EPC protocol than with the acknowledgement including the EPC code. The IF frequency sweep in Fig. 13 shows high variation of the read range, which are probably due to two reasons: First, the laboratory demonstrator measurement setup can give rise to standing waves and multipath propagation, effects that are enhanced by the higher carrier frequency. Secondly, the power of the up-converted RFID reader signal was frequency dependent, leading to manual adjustment of the output power of the RFID reader at every frequency point. Taking into account these non-idealities in the measurement setup, the measured results are in line with the simulated range.

V. Conclusion

This paper introduced a novel way to implement passive RFID at millimetre waves. The passive operation is achieved by adding an external mixing element between tag antenna and a standard RFID chip. The mixing element converts RFID reader signal from millimetre waves to RFID carrier frequency. The reader's TX and RX ports are similarly equipped with external mixers to convert the reader UHF output to millimetre waves and received signal millimetre wave signal to RFID carrier frequency.

The paper demonstrated the operation principle at 10 GHz with an EPC-compliant UHF tag IC. A Schottky diode was used as the mixing element. The diode achieved a measured conversion loss of -10 dB from millimetre waves to UHF at the operation power level of the tag. The tag was read using standard EPC reader up to 30 cm. The operation range can be extended to over a meter by using more sensitive RFID chips, e.g. semipassive chips, and in the future by using a capacitive mixing element, such as a varactor diode or a ferroelectric varactor.

Acknowledgments

The authors wish to thank Professors Alessandra Costanzo and Diego Masotti from University of Bologna for collaboration. We also thank Dr. Ville Viikari from VTT for fruitful discussion, and Ilkka Marttila from VTT for help during the measurements.

References

[1] EPC specifications, available at http://www.epcglobalinc.org/.
[2] ISO/IEC 18000-6 standard, available at http://www.iso.org.
[3] Jae Sung Choi; Hyun Lee; Elmasri, R.; Engels, D.W.; , "Localization Systems Using Passive UHF RFID," INC, IMS and IDC, 2009. NCM '09. Fifth International Joint Conference on , vol., no., pp.1727-1732, 25-27 Aug. 2009.
[4] Nikitin, P.V.; Martinez, R.; Ramamurthy, S.; Leland, H.; Spiess, G.; Rao, K.V.S.; , "Phase based spatial identification of UHF RFID tags," RFID, 2010 IEEE International Conference on , vol., no., pp.102-109, 14-16 April 2010.
[5] V. Viikari, P. Pursula, K. Jaakkola: Ranging of UHF RFID Tag Using Stepped Frequency Read-Out, accepted in IEEE Sensors Journal, December 2009.
[6] P. Pursula, T. Vähä-Heikkilä, A. Müller, D. Neculoiu, G. Konstantinidis, A. Oja, J. Tuovinen, "Millimetre Wave Identification — new radio system for low power, high data rate and short range", *IEEE Tr. on Microwave theory and techniques*, Vol. 56, No. 10, pp. 2221-2228, October 2008.
[7] D. Neculoiu, G. Konstantinidis, T. Vähä-Heikkilä, A. Müller, D. Vasilache, A. Stavinidris, L. Bary, M. Dragoman, I. Petrini, C. Buiculescu, Z. Hazoupulos, N. Kornilios, P. Pursula, R. Plana, D. Dascalu, "GaAs Membrane-Supported 60 GHz Receiver with Yagi-Uda Antenna," *MEMSwave 2007, 8th International Symposium on RF MEMS and RF Microsystems*, Barcelona, June 26-29 2007, pp. 15-18.
[8] F. Donzelli, V. Rizzoli, A. Costanzo and D. Masotti, "Integration of numerical and field-theorical techniques in the design of single- and multi-band rectennas for micro-power generation", accepted for publication in *International Journal of Microwave and Wireless Technologies*, 2010.
[9] S. Pellerano, J. Alvarado, Y. Palaskas, "A mm-wave power harvesting RFID tag in 90nm CMOS," *Custom Integrated Circuits Conference CICC*, pp.677-680, 13-16 Sept. 2009.
[10] Viikari, V.; Kantanen, M.; Varpula, T.; Lamminen, A.; Alastalo, A.; Mattila, T.; Seppa, H.; Pursula, P.; Saebboe, J.; Shi Cheng; Al-Nuaimi, M.; Hallbjorner, P.; Rydberg, A.; , "Technical Solutions for Automotive Intermodulation Radar for Detecting Vulnerable Road Users," Vehicular Technology Conference, 2009. VTC Spring 2009. IEEE 69th , vol., no., pp.1-5, 26-29 April 2009
[11] P. J. Gibson, "The Vivaldi aerial," in Proc. 9th European Microwave Conf., pp. 101–105, 1979.
[12] HFSS 3D Full-wave Electromagnetic Field Simulation.
[13] AWR-MWO Design Environment.
[14] V. Rizzoli, A. Costanzo, and G. Monti, "General electromagnetic compatibility analysis for nonlinear microwave integrated circuits", *2004 IEEE MTT-S Int. Microw. Symp. Digest*, pp. 953-956, June 2004.
[15] F. Donzelli, V. Rizzoli, P. Spadoni, A. Costanzo, D. Masotti and E.M. Vitucci, "A CAD Procedure for MIMO Link Estimation by the Combination of Nonlinear, Electromagnetic and Propagation Analysis Techniques", *2008 IEEE MTT-S Int. Microw. Symp. Dig.*, pp. 927-930, 2008.